Scientia Iranica, Vol. 10, No. 2, pp 227–237
© Sharif University of Technology, April 2003

SCIENTIA
IRANICA

A New Analytical Method for Evaluation of Energy Release Rate of a Fiber/Matrix Interfacial in Pull-Out Test

G. Karami* and P. Malekzadeh[1]

In this paper, a new model to obtain the Energy Release Rate (ERR) for pull-out test specimens, based on a variational approach, is introduced. To include radial dependency, due to axial deformations of a matrix, in an efficient and accurate way, a continuous displacement function is introduced which satisfies the required geometrical as well as kinetical boundary conditions. The displacement function includes the shear deformation. While obtaining the parameters of displacement function from the principle of total potential energy, two distinct solutions are recognized which have different physical interpretations. One solution demonstrates shear deformation and radial dependency, whereas the other solution represents a constant normal strain. Employing the proposed modeling, the effects of various geometrical and material parameters on ERR were studied. Numerical results are presented to show the accuracy and efficiency of this model in comparison with other such modelings.

INTRODUCTION

Different types of damage can occur in composite materials. Delamination, in particular, is very critical to laminated composites that have a low resistance to this failure mode, due to the inherent weakness of their interfaces. Initiation of a delamination has different sources such as: a) Low velocity impact [1], b) Structure free-edge effects [2-5] and c) Fabrication defects. Once the damage occurs, subsequent in-service loading may increase the delamination area, resulting in a stiffness decrease and an early failure of the part. Delamination may also cause a substantial loss in the load-carrying capacity of the structures [6,7].

The bonding between a fiber and the matrix is very important for the mechanicalbehavior of composites. It is shown that the quality of interface between the fiber/matrix plays the most important role in the development of different types of damage in composite fibrous materials [8,9]. By use of an axisymetric, cylindrical single fiber/matrix composite model, the fiber pull-out test is one of the four most commonly used methods for characterizing interfacial properties [10]. The debonding of matrix and fiber is a well-known fracture mechanics problem. Based on a continuum analysis of the deformation fields in cracked bodies, a singularity of some order will appear in the stress and strain tensor at the crack tip. Using a continuum mechanics approach, one can employ the theory of elasticity to evaluate the deformation field accurately. The fracture mechanics fundamentals are based on the change in the energy caused by incremental crack propagation. The energy change for an incremental growth in the crack, due to stress distribution in the singular region, is not considerable in comparison with the energy change in the regular region of the body. The strain energy of the regular region will not change considerably if the stresses are evaluated using the classical theory of mechanics of materials. Therefore, most of the research work being carried out to predict the fracture toughness in a pull-out test is, generally, based on the evaluation of the energy release rate using the classical approach (in which the singularity of the deformation field near the debonding region would not be considered). Some have employed the local form of equilibrium equations, which lead to a classical form of analysis based on the measured strains in the regions near to the crack tip of the cracked bodies (e.g. [11,12]). This approach also makes the base for the delamination phenomenon employed

*. *Corresponding Author, Department of Mechanical Engineering, School of Engineering, Shiraz University, Shiraz 71345, I.R. Iran.*

1. *Department of Mechanical Engineering, School of Engineering, Shiraz University, Shiraz 71345, I.R. Iran.*

by many researchers in laminated composite material analysis (e.g. [13,14]).

Among the many notable researchers, Chua and Piggot [15], Zhou et al. [11] and Piggot [16] have studied the fiber pull-out test and have predicted the stress distribution. Zhang [12] has used the stress function given by Kelly [17] and has derived a model for the strain energy release rate. In his analysis he has used the axial strain energy for both matrix and fiber, together with the shear strain energy for the matrix.

In conjunction with singular elements at the debonding or crack tip, finite elements (e.g. [18]) or boundary elements (e.g. [19,20]) elasticity analysis may also be employed with good accuracy for such problems.

In this paper, a new model to obtain the energy release rate in terms of the external applied stress is introduced. The principle of the total potential energy is used with good accuracy, in conjunction with an introduction of a new displacement function representing the deformation of both matrix and fiber. The displacement function includes, approximately, both the radial as well as the axial coordinate dependency of the deformation field. The effects of the various geometrical parameters on the strain energy release rate are studied. The results are compared with those of theoretical as well as experimental methods reported in [11,12,15,16].

DISPLACEMENT FUNCTION

In a single-fiber pull-out experiment, the matrix is kept fixed at one end ($x = 0$) and a tensile stress, σ, is applied at the other end ($x = L + L'$) of the embedded fiber (see Figure 1). The strain energy of this system is composed of two parts: One part is due to debonded fiber ($L \leq x \leq L + L'$) and the other part is due to the embedded fiber and the matrix ($0 \leq x \leq L$). The strain energy of the free fiber may be evaluated by the classical theory of the strength of the materials. The strain energy of the second part may be considered as the strain energy of fixed-ended embedded fiber and matrix minus the energy needed to keep the embedded fiber fixed (at $x = 0$). The energy to be evaluated is a function of the end displacement of the free fiber end (at $x = 0$) and also the stress distribution on the fixed fiber end (at $x = 0$). Due to the assumed continuity of the displacement at the interface, the displacement of the particles of the fiber at $r = r_f$ on the section $x = 0$ becomes zero. Considering this and also due to the fact that r_f is relatively small, the end displacement of the fiber is relatively small (see Figure 2). The work needed to keep the fiber end fixed at $x = 0$ is approximately:

$$W_e \cong \frac{1}{2} \int_{A_f} u_f(r,0)\sigma_f(r,0)dA_f, \tag{1}$$

where σ_f is the axial stress of the fiber, u_f is the axial displacement of the fiber, A_f is the cross sectional area of the fiber and W_e is the external work. A good approximate value for the normal stress at the fixed end is its mean value. Thus, Equation 1 becomes:

$$W_e \cong \frac{P}{2(A_f + A_m)} \int_{A_f} u_f(r,0)dA_f, \tag{2}$$

where A_m and A_f are the cross sectional areas of matrix and fiber, P is the axial load and W_e is the external work. The effects of the residual stresses may be superimposed to the other stresses. In order to evaluate the strain energy of the fixed embedded fiber and the matrix, a continuous displacement function, based on the following assumptions, is employed for the matrix and fiber. The assumptions are:

1. Due to applied stress in the axial direction (both shear and normal components), the strain energies are the dominants; thus, the strain energies, due to the hoop and radial components of the stress, may be neglected. This is because of the fact that the hoop and radial components of the stress are due to the Poisson effect. Moreover, for the problem under consideration, because of the loading condition (axial loading only) and geometry (relatively long specimens), the global effects on the strain energy are negligible. Also, it should be noted that the effect of radial displacement on axial shear strain

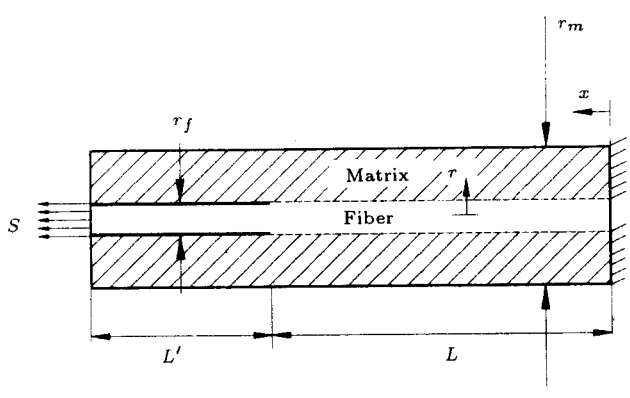

Figure 1. Geometry of the pull-out test specimen.

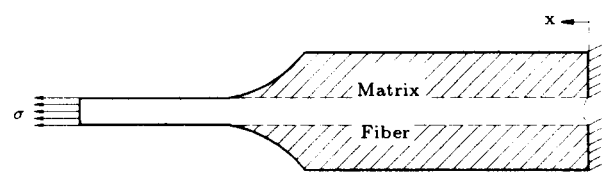

Figure 2. The deformed shape of the pull-out test specimen (the debonded matrix are not shown).

is insignificant. This is a common assumption that has been employed in [11,12,15]. In a mathematical sense, this assumption means that:

$$\frac{\partial \nu}{\partial x} = 0, \tag{3}$$

where ν is the radial component of the displacement and x is the axial coordinate variable.

2. Since the fiber radius is very small in comparison with the fiber length, the radial dependency of its axial displacement is neglected.

A continuous displacement function, that includes the radial dependency of the matrix axial displacement, is assumed for the whole body as:

$$u(x,r) = X(x) + H(\zeta)R(\zeta)X(x), \quad \text{with} \quad \zeta = \frac{r}{r_f} - 1. \tag{4}$$

Here, u is the axial displacement, $H(\zeta)$ is the heavisides unit step function, $X(x)$ is an unknown function of the axial coordinate and $R(\zeta)$ represents the radial dependency of the displacement of the matrix. The function $R(\zeta)$ should satisfy some geometrical and kinetical requirements.

Geometrical Conditions

The displacement function must be such that the continuity of displacements, in axial direction, at the interface between the fiber and matrix, is satisfied. This means that:

$$u(x,r^-) = u(x,r^+). \tag{5}$$

Kinetical Conditions

a) The shear stress at the outer surface of the matrix must be zero, whereas at the interface of the matrix and fiber it is nonzero. These requirements, in the mathematical form, can be stated as:

$$G_m\left(\frac{\partial u}{\partial r}\right)\Big|_{\zeta=\zeta_m} = 0, \tag{6a}$$

$$G_m\left(\frac{\partial u}{\partial r}\right)\Big|_{\zeta=0^+} \neq 0. \tag{6b}$$

b) The shear stress must decrease monotonically in a given section in a radial direction. Thus, to satisfy the above requirements, the following expression for function $R(\zeta)$ has been chosen:

$$R(\zeta) = A[\zeta - (1+\zeta_m)\ell n(1+\zeta)], \tag{7}$$

where $\zeta_m = \frac{r_m}{r_f} - 1$. A is an unknown parameter that should be determined. It can easily be shown that Equation 7 satisfies all the requirements stated above. The parameter A and the function $X(x)$ would be determined from the principle of the total potential energy. In the next section, the basic governing equations required to derive the expression for the total potential energy of the system are described.

BASIC GOVERNING EQUATIONS

Kinematics

The strain components of both the matrix and fiber can be derived from the general strain-displacement relations. The non-zero components, i.e. the components that can be derived from the axial displacements without applying the stresses, are:

1. The axial component:

$$\varepsilon_x = \frac{\partial u}{\partial x} = \frac{dX}{dx}(1+H(\zeta)R(\zeta)) = X'(1+H_{(\zeta)}R_{(\zeta)}), \tag{8}$$

2. The shear strain in matrix:

$$\gamma_{xr} = \frac{\partial u}{\partial r} = XH\frac{dR(\zeta)}{dr} = XHR'(\zeta)\frac{1}{r_f}. \tag{9}$$

Kinetics

Constitutive Equations

The relations between the stress and strain components for an elastic material are:

$$\varepsilon_x = \frac{1}{E}[\sigma_x - \nu(\sigma_r + \sigma_\theta)],$$

$$\varepsilon_r = \frac{1}{E}[\sigma_r - \nu(\sigma_x + \sigma_\theta)],$$

$$\varepsilon_\theta = \frac{1}{E}[\sigma_\theta - \nu(\sigma_r + \sigma_x)],$$

$$\gamma_{xr} = \frac{\tau_{xr}}{G}. \tag{10}$$

These equations may be used for both fiber and matrix.

The Strain Energy

In a general form, the strain energy for an elastic body is given as [21,22]:

$$U = \int_\nu \left[\frac{1}{2E}(\sigma_x^2+\sigma_\theta^2+\sigma_r^2) + \frac{1}{2G}(\tau_{r\theta}^2+\tau_{xr}^2+\tau_{x\theta}^2)\right] d\nu. \tag{11}$$

Under the prescribed assumptions, Equation 11 takes the following form:

$$U = U_m + U_f = \int_{\nu_m}\left[\frac{E_m\varepsilon_x^2}{2} + \frac{G_m\gamma_{xy}^2}{2}\right] d\nu + \int_{\nu_f}\left(\frac{E_f}{2}\varepsilon_x^2\right) d\nu, \tag{12}$$

where U_m and U_f are the matrix and fiber strain energy, respectively. Substituting for the strain components from Equations 10, the strain energy of the fiber and matrix become, respectively:

$$U_f = \int_0^L \frac{E_f A_f}{2} X'^2 dx, \tag{13}$$

$$U_m = \int_0^L \int_{r_f}^{r_m} \left[\frac{E_m}{2}(1+R)^2 X'^2 + \frac{G_m}{2r_f^2}(XR')^2\right] 2\pi r dr dx. \tag{14}$$

The total strain energy of the system, then, becomes:

$$U = \int_0^L [\alpha X'^2 + \beta X^2] dx, \tag{15}$$

where:

$$\alpha = \frac{E_f A_f}{2} + \frac{E_m A_f}{2}(2\zeta_m + \zeta_m^2 + 4A\gamma_m + 2A^2 I^*), \tag{16a}$$

$$\beta = \pi A^2 G_m \beta_m, \tag{16b}$$

γ_m, I^*, β_m in Equations 16 are given in Appendix A.

Principle of Total Potential Energy

The total potential energy is composed of the strain energy and the potential energy of the external forces that are conservative in the problem under study, as:

$$\Pi = U + V, \tag{17}$$

where V is the potential energy of the external applied loads. In the problem under consideration, one has only the work of the load applied at the end of the embedded fiber ($x = L$). Based on the principle of total potential energy for a conservative system, Π must be stationary in an equilibrium state. Thus:

$$\delta\Pi = \delta U + \delta V = 0, \tag{18}$$

where, δV is equal to the virtual work of the external applied load with an opposite sign; therefore:

$$\delta V = -P\delta X(L). \tag{19}$$

Using Equations 15, 18 and 19 and carrying out the integration by part, the following results are obtained:

$$\delta X : X'' - \frac{\beta}{\alpha} X = 0, \tag{20}$$

$$\delta A : \int_0^L [X'^2 \frac{\partial \alpha}{\partial A} + X^2 \frac{\partial \beta}{\partial A}] dx = 0, \tag{21}$$

$$\delta X(L) : X'(L) = \frac{P}{2\alpha}. \tag{22}$$

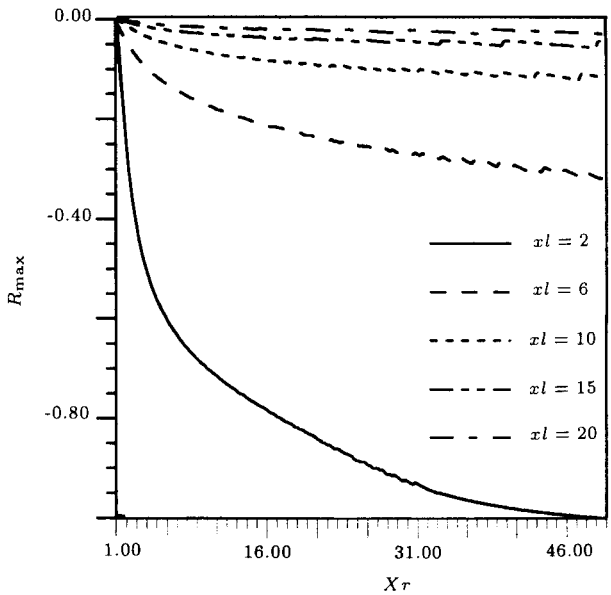

Figure 3. The variation of the maximum value of the function $R(r)$ with $Xr(=\frac{r_m}{r_f})$ ($E_f = 1258.6$ and $E_m = 3.4$ GPa).

From Equations 16a and 16b, it is obtained that, respectively:

$$\frac{\partial \alpha}{\partial A} = 2A_f E_m(\gamma_m + AI^*) = \alpha_0, \tag{23a}$$

$$\frac{\partial \beta}{\partial A} = 2\pi A G_m \beta_m = \beta_0. \tag{23b}$$

The solution of Equation 20 with the associated boundary conditions becomes:

$$X(x) = A_0 \sinh(\lambda x), \tag{24}$$

where, $\lambda = \sqrt{\frac{\beta}{\alpha}}$ and $A_0 = \frac{P}{2\alpha\lambda}$. To obtain the solution $X(x)$, it is required to know the value of the parameter A, which may be obtained from Equation 21. Substituting for $X(x)$ from Equation 24, Equation 21 takes the following form:

$$\frac{\eta - 1}{\eta + 1} + \frac{\sinh(2\lambda L)}{2\lambda L} = 0, \tag{25}$$

with $\eta = \frac{\alpha_0 \beta}{\beta_0 \alpha}$. Now A may be evaluated by solving Equation 25. Since the second term in Equation 4, i.e. $H(\zeta)R(\zeta)X(x)$, represents the radial dependency of the displacement function in the matrix, it should be always negative. $X(x)$ and $H(\zeta)$ are positive. In Equation 7, the term multiplied by A is always negative. Hence, it should be concluded that A must be always positive. In Figure 3, the variations of A are plotted versus the $xl(=\frac{L}{r_m})$ of the specimen for three different values of xl.

STRAIN ENERGY RELEASE RATE

One of the well accepted criteria for the crack propagation phenomenon is the total energy release rate, G_T, which can be derived from the change of strain energy of the body, U, with respect to the crack length, a, as [23-27]:

$$G_T = \frac{\partial U}{\partial a}. \tag{26}$$

For the problem under consideration, U is composed of three terms:

1. The strain energy of the free fiber, $U_1 = \frac{P^2 L'}{2A_f E_f}$,
2. The strain energy of the embedded fiber and the matrix (with a fixed-end boundary condition for both fiber and matrix), which can be evaluated from Equations 15 and 24 as:

$$U_2 = \frac{\beta A_0^2}{2\lambda} \sinh(2\lambda L), \tag{27}$$

3. The third component is due to the end effect at $x = 0$. As stated previously, since the specimen is fixed at the fiber end ($x = 0$), the strain energy of the system, due to this end effect, should be recovered. This effect was proved to be equal to W_e. Thus, $U_3 = -W_e$ must be added to U_2.

The total strain energy of the system, U_T, is, therefore, the sum of U_1, U_2 and U_3. The total strain energy release rate can, then, be derived using Equations 26 and 27 as:

$$G_T = \frac{1}{2\pi r_f} \frac{dU_T}{dL'}. \tag{28}$$

Thus:

$$G_T = \frac{1}{2\pi r_f}\left[\frac{d}{dL'}\left(\frac{P^2 L'}{2A_f E_f} - \frac{P^2}{4\alpha}\text{sech}^2(\lambda L)\right) - \frac{dW_e}{dL'}\right]. \tag{29}$$

Note that, $\frac{d()}{dL'} = -\frac{d()}{dL}$. For a detailed differentiation of U_2, see Appendix B. W_e depends on the displacement and stresses at the end $x = 0$. $u_f(0,r)$ and $\sigma_f(0,r)$ become independent of the length, L, when L is relatively long in comparison with r_f. This does not mean that the effects of the boundary condition at $x = 0$ on the body, at a distance far from the end, may be neglected, it rather means that these effects are, approximately, independent of a small change in the length, L, for a long L. Therefore, the change of W_e, with respect to change of length, L, is very small and, in comparison with the other terms in Equation 29, may be neglected. By neglecting the third term in Equation 29 and by using the relation between the applied stress and load P, the NERR (Normalized Energy Release Rate) becomes:

$$\begin{aligned}\overline{G}_T &= 1 - \frac{\partial}{\partial L}\left[\frac{\tanh(\lambda L)}{\lambda\overline{\alpha}}\right] \\ &= 1 - \frac{\tanh(\lambda L)}{(\lambda L)\overline{\alpha}} - L\frac{\partial}{\partial L}\left[\frac{\tanh(\lambda L)}{(\lambda L)\overline{\alpha}}\right] \\ &= 1 - \frac{\tanh(\lambda L)}{(\lambda L)\overline{\alpha}} - Lg,\end{aligned} \tag{30}$$

where:

$$\overline{\alpha} = 1 + (\frac{E_m}{E_f})(2\zeta_m + \zeta_m^2 + 4A\gamma_m + 2A^2 I^*),$$

$$g = \frac{\partial}{\partial L}\left[\frac{\tanh(\lambda L)}{(\lambda L)\overline{\alpha}}\right].$$

G_T is normalized according to [14]:

$$\overline{G}_i = \frac{G_i}{(\sigma^2 r_f / 4E_f)}.$$

The third term in Equation 30 has no considerable effect when the embedded length is large in comparison with the matrix radius, since the variation of parameter A, with respect to L is very small (see Figure 3). However, in current analysis, this effect has been accounted for. The variation of $(\frac{\tanh(\lambda L)}{\lambda L})$, with respect to L, is small, since the term λL is small. The differentiation to evaluate g is shown in Appendix B.

NUMERICAL RESULTS

The effects of geometrical parameters (ζ_m and $xl = L/r_m$) and material parameters ($e = E_m/E_f$) are studied on the Normalized Energy Release Rate (NERR). To start the analysis, one should first solve Equation 25 to obtain the values of parameter A for a given situation. There are two values for parameter A, irrespective of the geometrical and material parameters. One solution is $A = A_1 = 0$, which causes the displacement function $u(x,r)$ to become independent of radial coordinate r. The physical interpretation of such a solution is that one can solve the problem with constant strain throughout the embedded length. In this solution, the end effects are not important since the strains are constant. The NERR obtained from this solution is exactly equal to those obtained by Zhou et al. [11]. To check this point, when a approaches zero, Equation 30 becomes:

$$\overline{G}_T = 1 - \frac{1}{1 + e(2\zeta_m + \zeta_m^2)} = \frac{e}{X + e}, \tag{31}$$

with $X = \frac{r_f^2}{r_m^2 - r_f^2}$. Equation 31 is identical to Equation 25 of [12]. This value of NERR is dependent on the

embedded length. It is easily seen from this equation that the limiting (maximum) value of $\overline{G}_T$ approaches 1. The solution of Equation 25 depends on both the geometrical and material properties of the specimen. Here, the other solution of Equation 25 is referred to as A_2. This value causes $R(r)$ to become nonzero and, therefore, the radial dependencies are present in the deformation pattern. In Figure 4, the variation of the maximum value of function $R(r)$ is plotted. The value of parameter A decreases as ζ_m increases but R_m increases with an increase in ζ_m. The NERR obtained from this value of A, i.e. A_2 contains the effects of the radial dependency of the deformation fields. In Figures 5a to 5h, the variation of $\overline{G}_T$ are plotted as a function of $Xr(Xr = r_m/r_f)$, for different values of the embedded length and for different materials for the fiber and matrix. The results are compared with those of Kim et al. [28] and Zhou et al. [11]. The NERR given by Kim et al. or Zhou et. al is presented by:

$$G_T = \frac{(1-2k\nu_f)^2}{[(1-2k\nu_f)+\frac{X}{e}(1-2k\nu_f)]}\frac{\sigma^2 r_f}{4E_f}, \qquad (32)$$

with $k = \frac{e\nu_f + X\nu_m}{e(1-\nu_f)+1+\nu_m+2X}$. Equation 32 contains the effects of the radial and hoop stresses in the regular region. The results of this modeling indicate that these effects are negligible, since the results for $A_1 = 0$ and A_2 are in close agreement with the results given by Equation 32. In Equations 31 and 32, the effect of length is not a parameter to be considered. However, the results show that only when the embedded length is large enough in comparison with r_m, one can conclude that NERR is independent of the length. This conclusion may be made from

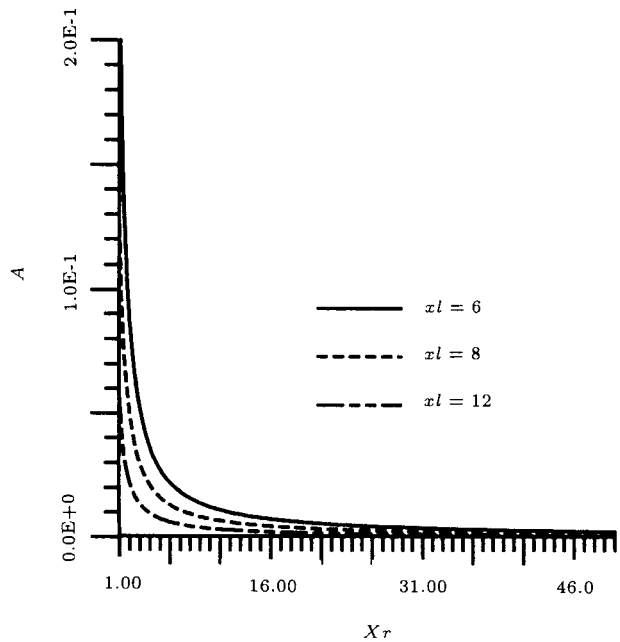

Figure 4. The variation of parameter A, with xl and Xr.

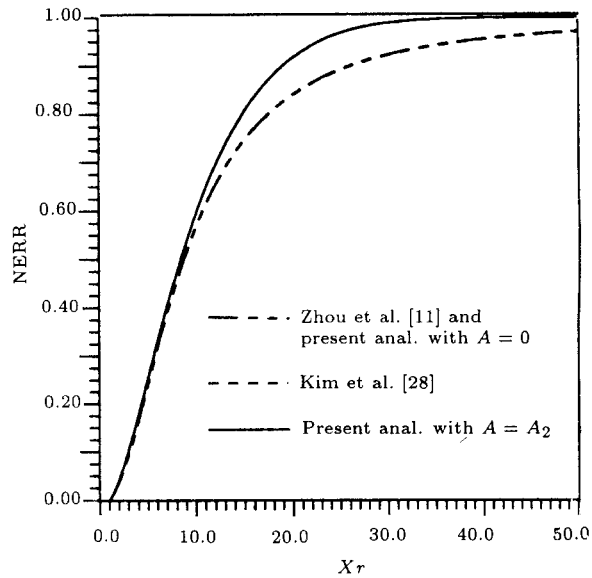

Figure 5a. Change of NERR with $Xr(=\frac{r_m}{r_f})$ $(xl = 2, E_f = 258.6$ and $E_m = 3.4$ Gpa).

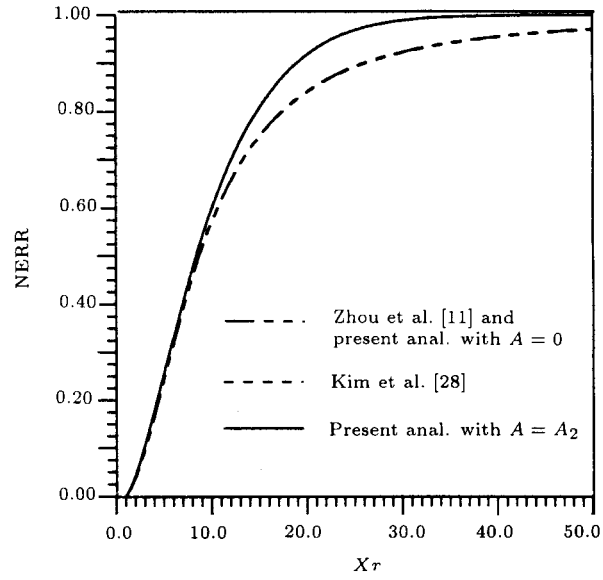

Figure 5b. Change of NERR with $Xr(=\frac{r_m}{r_f})$ $(xl = 2, E_f = 150.6$ and $E_m = 3.95$ Gpa).

Figures 6a to 6c. In Figure 6a, the values of NERR are compared for three different intermediate embedded lengths. From these figures it is also clear that in addition to length independency, the radial effects are also negligible when xl becomes large. In Figures 7a and 7b the values for the parameter A are plotted.

Although one can see that A takes different values for different lengths, NERR becomes approximately independent of the length, which means that the shear effect is negligible when xl becomes large, irrespective of ζ_m. Another important observation which may be made is the effects of the end condition at $x = 0$.

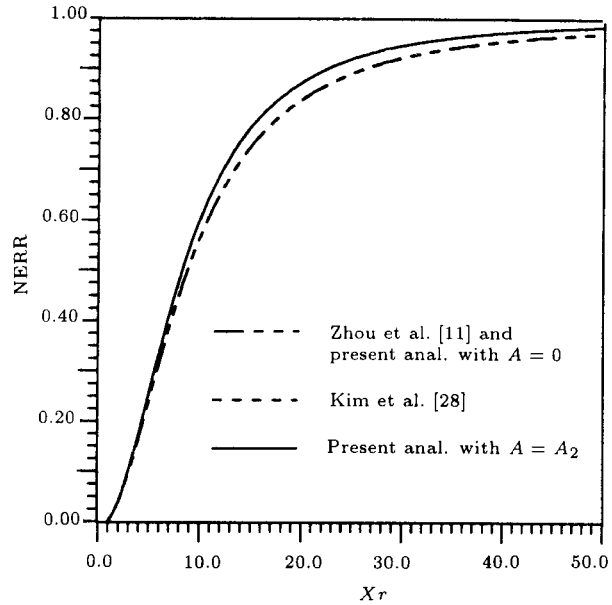

Figure 5c. Change of NERR with $Xr(=\frac{r_m}{r_f})$ ($xl = 6, E_f = 258.6$ and $E_m = 3.4$ Gpa).

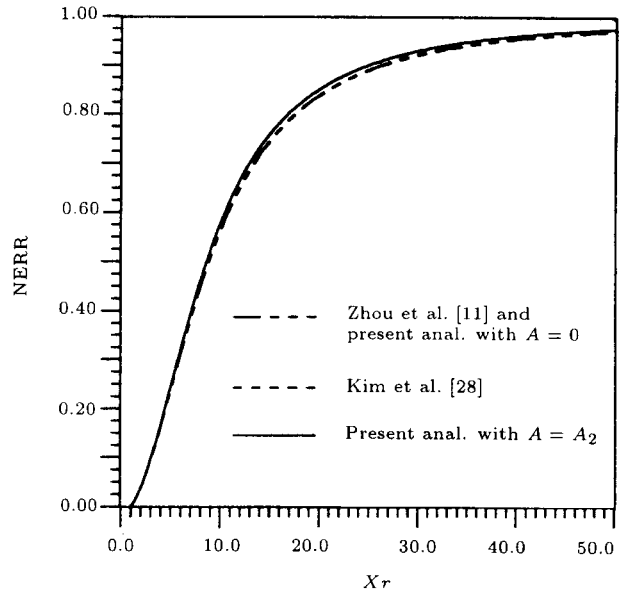

Figure 5e. Change of NERR with $Xr(=\frac{r_m}{r_f})$ ($xl = 10, E_f = 258.6$ and $E_m = 3.4$ Gpa).

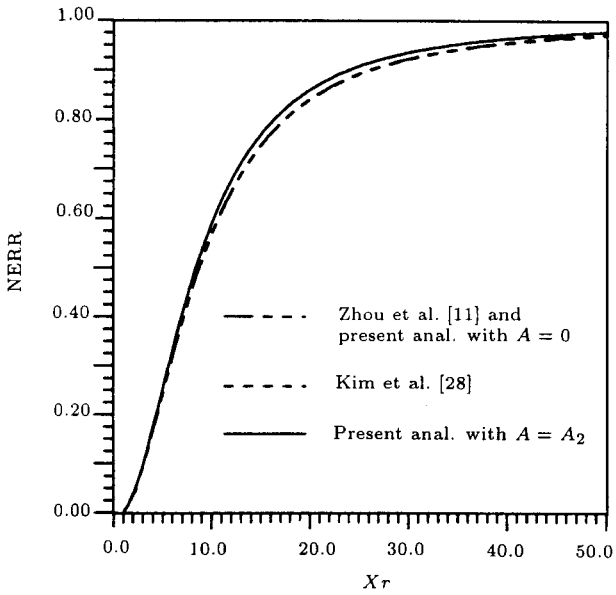

Figure 5d. Change of NERR with $Xr(=\frac{r_m}{r_f})$ ($xl = 8, E_f = 258.6$ and $E_m = 3.4$ Gpa).

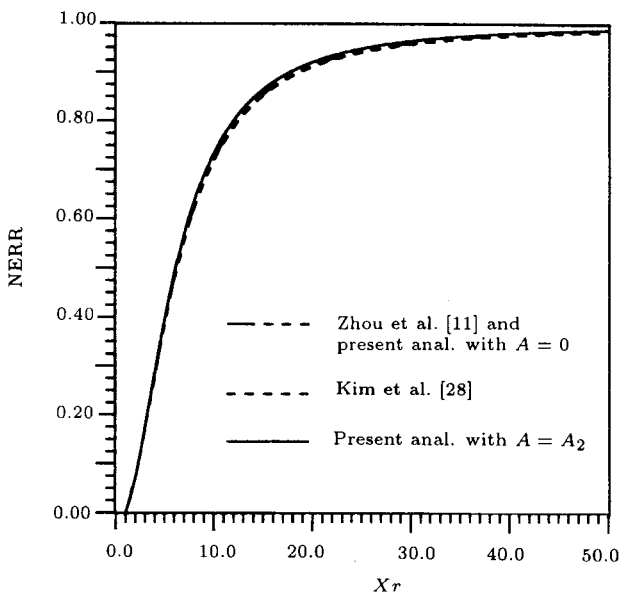

Figure 5f. Change of NERR with $Xr(=\frac{r_m}{r_f})$ ($xl = 10, E_f = 150.6$ and $E_m = 3.4$ Gpa).

From the results obtained, one can see that NERR is less sensitive to the end effect. This does not mean that the end effect has no contribution on the deformation pattern, but that, its effect due to a small change in the embedded length is negligible. The mechanism of the fracture would be changed with an increase in ζ_m, i.e., for small values of ζ_m, mode II of the fracture is the dominant mode. As ζ_m increases, mode I becomes the dominant mode tending to the situation of plain strain condition which, subsequently, causes an increase in G_I and, hence, in total energy release rate. By considering the shear effect, NERR tends to increase. This is because an increase in the total strain energy of the system occurs and the energy required for an infinitesimal increase in the crack length can be obtained with no changes in the deformation pattern of the body.

In Table 1, the results for NERR are compared with those obtained for the identical problem presented by other researchers. It seems that the modeling presented in this work yields more accurate results (especially when considering A_2 solutions) than those results given by Zhang [12] and Chua and Piggot [15].

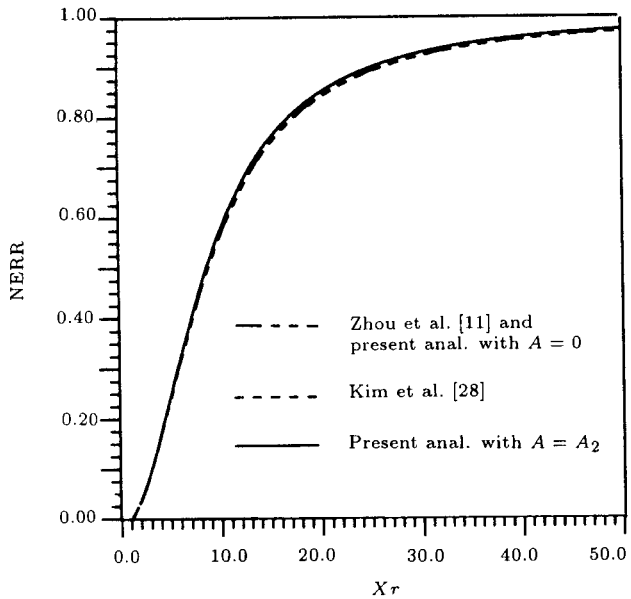

Figure 5g. Change of NERR with $Xr(=\frac{r_m}{r_f})$ ($xl = 12, E_f = 258.6$ and $E_m = 3.4$ Gpa).

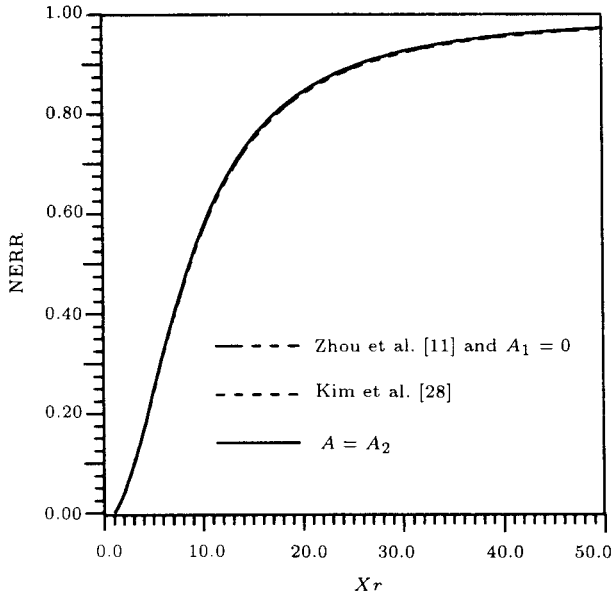

Figure 5h. Change of NERR with $Xr(=\frac{r_m}{r_f})$ ($xl = 20, E_f = 258.6$ and $E_m = 3.4$ Gpa).

Comparative calculations have been conducted for the material parameters pertinent to carbon/epoxy: $E_f = 258.6$ GPa, $E_m = 3.4$ GPa, $\nu_f = 0.25$ and $\nu_m = 0.35$, $L = 130$ mm, $r_f = 4.5$ mm, $r_m = 16.2$ mm.

CONCLUSIONS

A new modeling for the debonding and fiber pull-out interfacial fracture energy was presented. In the modeling, a displacement function is introduced and the principle of total potential energy is employed to determine the energy release rate. The solution includes the radial dependency of the deformation pattern. The analysis shows that the radial and hoop stresses under the applied load have negligible effects on NERR. The effect of shear deformation becomes small for two cases: When the radius of matrix is not larger than the radius of fiber and when the embedded length becomes very large in comparison with the matrix radius. The effects of the geometrical and material properties were studied on NERR. The results have shown that since, in a pull-out test, the embedded length is usually

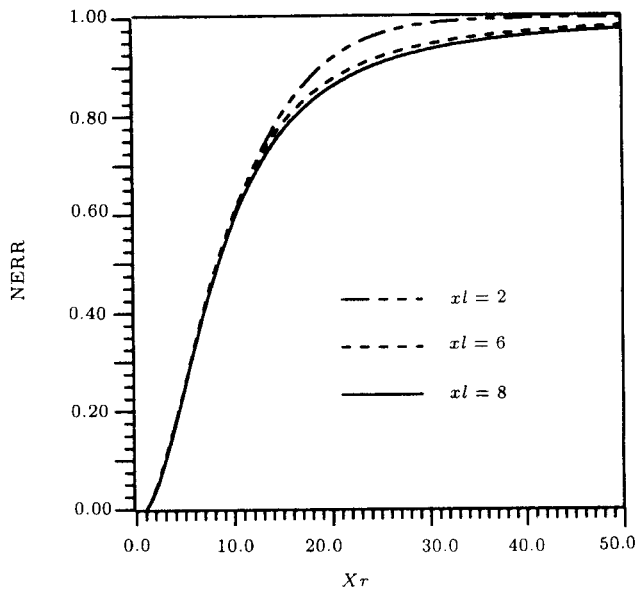

Figure 6a. Comparisons of normalized energy release rate versus Xr for three intermediate xl ($E_f = 258.6$ and $E_m = 3.4$ GPa).

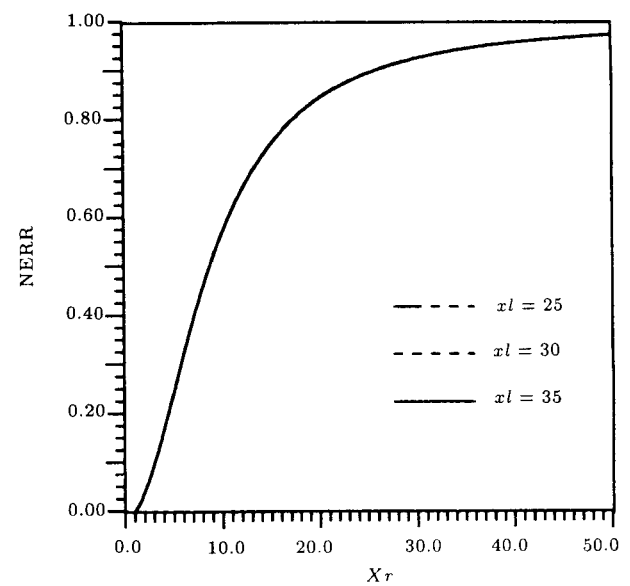

Figure 6b. Comparisons of normalized energy release rate versus Xr for three large xl ($E_f = 258.6$ and $E_m = 3.4$ GPa).

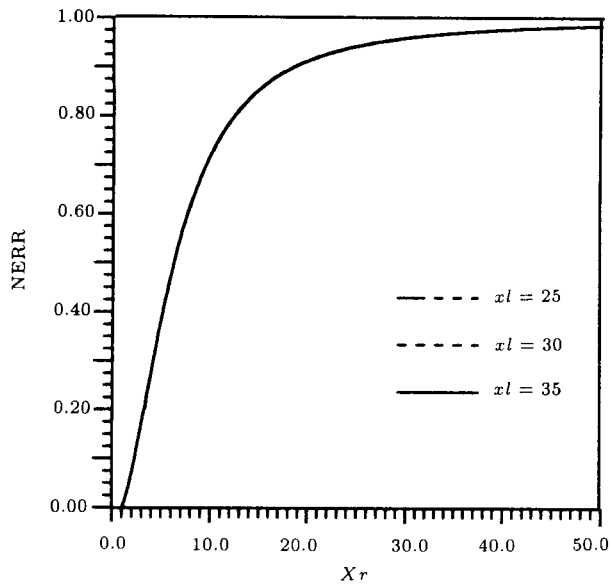

Figure 6c. Comparisons of normalized energy release rate versus Xr for three large xl ($E_f = 150.6$ and $E_m = 3.95$ GPa).

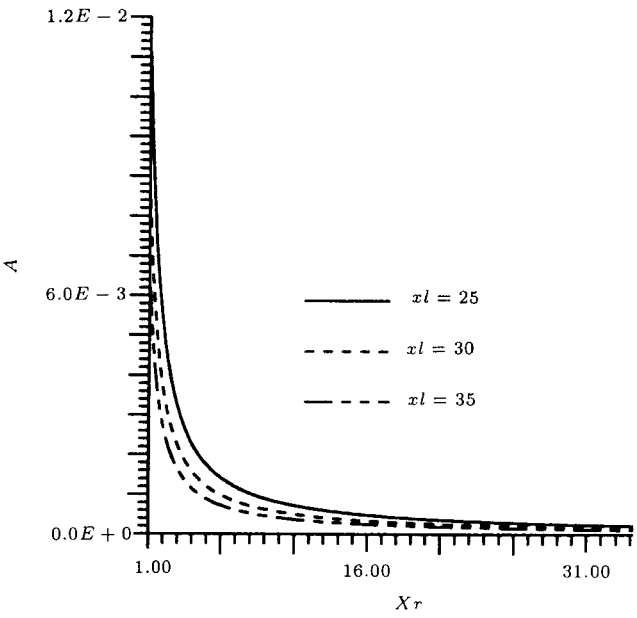

Figure 7a. The variation of parameter A, with respect to xl and Xr($E_f = 258.6$ and $E_m = 3.4$ GPa).

much larger than the matrix radius, neglecting the radial dependency would not introduce significant errors.

Table 1. Comparisons of NERR results from different modelings.

Zhang et al. [12]	Chua and Piggot [15]	Kim et al. [28]	Present Work Eq. 31 A = 0	Present Work Eq. 30 A = A_2
0.188	0.403	0.135	0.134	0.140

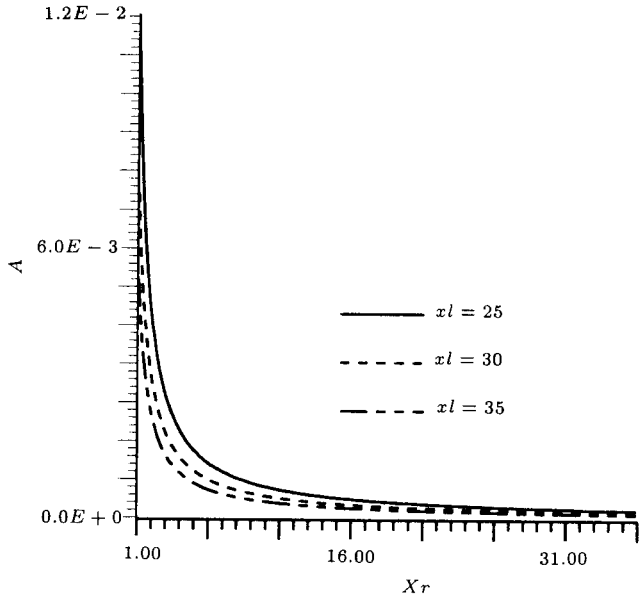

Figure 7b. The variation of parameter A, with respect to xl and Xr($E_f = 150.6$ and $E_m = 3.95$ GPa).

REFERENCES

1. Greszczuk, L.B. "Damage in composite materials due to low-velocity impact", in *Impact Dynamics*, L.A. Zukas, Ed., John Wiley, New York, USA (1982).
2. Spilker, R.L. "Edge effects in symmetric composite laminates: importance of satisfying the traction-free-edge condition", *J. Comp. Mats*, **14**, pp 2-20 (1980).
3. Davidson, B.D. "Energy release rate determination for edge delamination under combined in-plane, bending and hydrothermal loading. Part II -Two symmetrically located delaminations", *J. Comp. Mat.*, **128**(14), pp 1371-1392 (1994).
4. Rybicki, E.F., Schmueser, D.W., and Fox, J. "An energy release rate approach for stable crack growth in the free edge delamination problems", *J. Comp. Mat.*, **11**, pp 470-487 (1977).
5. Kaczmarek, K., Wisnorm, M.R. and Jones, M.I. "Edge delamination in curved (Glass-fiber/epoxy beams loaded in bending", *Comp. Sci. Tech.*, **58**, pp 155-161 (1998).
6. Simitses, G.J., Sallam, S. and Yin, W.L. "Effect of delamination of axially loaded homogeneous laminated plates", *AIAA J.*, **23**(9), pp 1437-1445 (1985).
7. Yin, W.L., Sallam, S.N. and Simitses, G.J. "Ultimate axial load capacity of a delaminated beam-plate", *AIAA J.*, **24**(1), pp 123-129 (1986).
8. Albertsen, H., Ivens, J., Peters, P., Wevers, M. and Verpoest, I. "Interlaminar fracture toughness of cfrp influenced by fiber surface treatment: Part 1. Experimental results", *Comp. Sci. Tech.*, **54**, pp 133-145 (1995).
9. Ivens, J., Albertsen, H., Wevers, M., Verpoest, I. and Peters, P. "Interlaminar fracture toughness of cfrp influnced by fiber surface treatment: Part 2. Modeling

of the interface effect", *Comp. Sci. Tech.*, **54**, pp 147-159 (1995).

10. Pithkethly, M.J. et al. "A round-robin program on interfacial test methods", *Comp. Sci. Tech.*, **48**, pp 1205-214 (1993).
11. Zhou, L.M., Kim, J.K. and Mai, Y.W. "Interfacial debonding and fiber pull-out stresses, Part II. A new model based on the fracture mechanics approach", *J. Mat. Sci.*, **27**, pp 3155-3166 (1992).
12. Zhang, S.Y. "A new model for the energy release rate of fiber/matrix interfacial fracture", *Comp. Sci. Tech.*, **54**, pp 163-166 (1998).
13. Kardomateas, G.A. and Chung, C.B. "Thin film modeling of delamination buckling in pressure loaded laminated cylindrical shells", *AIAA J.*, **30**(8), pp 2119-2122 (1992).
14. Zheng, S. and Sun, C.T. "Delamination interaction in laminated structures", *Eng. Fracture Mech.*, **59**(2) pp 225-240 (1998).
15. Chua, P.S. and Piggot, M.R. "The glass fiber-polymer interface, I. theoretical consideration for single fiber pull-out tests", *Comp. Sci. Tech.*, **22**, pp 33-42 (1985).
16. Piggot, M.R. "Debonding and friction at fiber-polymer interfaces, I. criterion for failure and sliding", *Comp. Sci. Tech.*, **30**, pp 295-306 (1987).
17. Kelly, A., *Strong Solids*, 2nd Edn., Clarendon Press, Oxford, UK (1973).
18. Lammerant, L. and Verpoest, I. "Modeling of the interaction between matrix cracks and delaminations during impact of composite plates", *Comp. Sci. Tech.*, **56**, pp 1171-1178 (1996).
19. Karami, G. and Fenner, R.T. "Analysis of mixed mode fracture and crack closure using the boundary integral equation method", *Int. J. Fracture*, **30**, pp 15-31 (1986).
20. Karami, G. "Multi-domain boundary element modeling of crack closure problems", in *Boundary Element X*, **2**, Stress Analysis, Brebbia, C.A., Ed., Springer-Verlag, Berlin, Germany (1988).
21. Shames, I.H. and Dyme, C.L., *Solid Mechanics, A Variational Approach*, Prentice-Hall, London, UK (1973).
22. Langhar, *Energy Methods in Applied Mechanics*, John-Wiley and Sons (1962).
23. Chybanbin, H., Kao, C.J. and Chang, L.E. "Delamination fracture criteria for composite laminates", *J. Comp. Mat.*, **29**, pp 1962-1987 (1995).
24. Singh, "Mixed mode fracture in an interleaved carbon-fiber/epoxy composite", *Comp. Sci. Tech.*, **55**, pp 319-327 (1995).
25. Davidson, B.D. et. al. "Three-dimensional analysis of center- delaminated unidirectional and multidirectional single-leg bending specimens", *Comp. Sci. Tech.*, **54**, pp 385-394 (1995).
26. Rybicki, E.F.U. "Mode I and mixed mode energy release rate values for delamination of graphite/epoxy test specimens", *J. Comp. Mat.*, **21**, pp 05-123 (1987).
27. Meguid, S.A. "Engineering Fracture Mechanics", *Elsevier Applied Science* (1989).
28. Kim, J.K. and Mai, Y.W. "Interfacial debonding and fiber pull-out stresses, Part I. Critical comparison of existing theories with experiments", *J. Mater Sci*, **27**, pp 3143-3154 (1992).

APPENDIX A

$$I^* = \int_0^{\zeta_m} [\zeta^2 + (1+\zeta_m)^2 \ln^2(1+\zeta) - 2\zeta(1+\zeta_m)\ln(1+\zeta)](1+\zeta)d\zeta$$

$$= \frac{\zeta_m^3}{3} + \frac{\zeta_m^4}{4} + (1+\zeta_m)^2 A_1 - 2(1+\zeta_m)A_2 + 2(1+\zeta_m)A_3,$$

where:

$$A_1 = \int_0^{\zeta_m} (1+\zeta)\ln^2(1+\zeta)d\zeta$$

$$= \frac{(1+\zeta_m)^2}{2}[\ln^2(1+\zeta_m) - \ln(1+\zeta_m) + 0.5] - 0.25,$$

$$A_2 = \int_0^{\zeta_m} (1+\zeta)^2 \ln(1+\zeta)d\zeta$$

$$= \frac{(1+\zeta_m)^3}{3}[\ln(1+\zeta_m) - 0.1/3] + +1/9,$$

$$A_3 = \int_0^{\zeta_m} (1+\zeta)\ln(1+\zeta)d\zeta$$

$$= \frac{(1+\zeta_m)^2}{2}[\ln(1+\zeta_m) - 0.5] + 0.25,$$

The β_m is given by:

$$\beta_m = \int_0^{\zeta_m} [\zeta - 2\zeta_m - 1 + \frac{(1+\zeta_m)^2}{1+\zeta}]d\zeta$$

$$= (1+\zeta_m)^2 \ln(1+\zeta_m) - \zeta_m(1 + \frac{3\zeta_m}{2}).$$

The parameter γ is given as:

$$\gamma = (\frac{2A_f}{A_m}) \int_0^{\zeta_m} (1+\zeta)R(\zeta)d\zeta$$

$$= (\frac{2A_f}{A_m}) \int_0^{\zeta_m} [\zeta - (1+\zeta_m)\ln(1+\zeta)](! + \zeta)d\zeta$$

$$= (\frac{2AA_f}{A_m})[\frac{4(3\zeta_m^2 + 2\zeta_m^3) + 6(\zeta_m^2 + 2\zeta_m)(1+\zeta_m)}{24}$$

$$- \frac{(1+\zeta_m)^3}{2}\ln(1+\zeta_m)]$$

$$= (\frac{2AA_f}{A_m})\gamma_m.$$

APPENDIX B

To evaluate g in Equation 31 it is required to obtain $\frac{\partial A}{\partial L}$. From Equation 25 one has, after taking the logarithm of each sides of the equation,

$$-\frac{\partial \eta}{\partial L}(\frac{2}{1-y_1^2}) = \frac{\partial x}{\partial L}(\cot anh(x) - \frac{1}{x}) = \frac{\partial x}{\partial L}\eta_1, \tag{B1}$$

where, $x = 2\lambda L$. Also, from Equation 25, it is noted that $\eta = \frac{\alpha_0 \beta}{\beta_0 \alpha}$. Therefore:

$$\frac{\partial \eta}{\partial L} = \eta[(\gamma_m + 2AI^*)/(\gamma_m A + A^2 I^*)$$

$$- 4e(\gamma_m + AI^*)/\overline{\alpha}]\frac{\partial A}{\partial L} = \eta\eta_2 \frac{\partial A}{\partial L}. \tag{B2}$$

Also, from Equation 24, the following is obtained:

$$\frac{\partial \lambda}{\partial L} = \lambda[\frac{1}{A} - 2e(\gamma_m + AI^*)/\overline{\alpha}]\frac{\partial A}{\partial L}$$

$$= \lambda\eta_3 \frac{\partial A}{\partial L}. \tag{B3}$$

Using Equations B1 to B3, $\frac{\partial A}{\partial L}$ is determined as:

$$\frac{\partial A}{\partial L} = \frac{-\eta_1 \lambda}{(\eta_2 + \eta_1\eta_3)L}. \tag{B4}$$

From Equation 25, the following is obtained:

$$g = \frac{\partial}{\partial L}[\frac{\tanh(\lambda L)}{(\lambda L)\overline{\alpha}}]$$

$$= [\frac{\sec h^2(\lambda L)}{\tanh(\lambda L)}(\frac{1}{2}\frac{\partial x}{\partial L}) - \frac{(\frac{\partial \lambda}{\partial L})}{\lambda} - \frac{(\frac{\partial \overline{\alpha}}{\partial L})}{\alpha} - 1][\frac{\tanh(\lambda L)}{(\lambda L)\overline{\alpha}}]. \tag{B5}$$

Using Equations B1 to B4, g can be obtained from Equation B5.